

# A new model for calculating specific resistance of aggregated colloidal cake layers in membrane filtration processes

Albert S. Kim\*, Rong Yuan

*Department of Civil and Environmental Engineering, University of Hawaii at Manoa, 2540 Dole Street, Honolulu, HI 96822, USA*

Received 2 December 2003; received in revised form 20 August 2004; accepted 25 August 2004

Available online 18 November 2004

## Abstract

A simple model to evaluate hydrodynamic cake resistance due to filtered aggregates is developed in this study. An aggregate is treated as a hydrodynamically as well as geometrically equivalent solid core with a porous shell. Creeping flow past a swarm of the composite spheres is solved using Stokes' equation and Brinkman's extension of Darcy's law. The dimensionless drag force ( $\Omega$ ) exerted on the composite sphere is analytically determined by four parameters: radius of the solid core, thickness of the porous shell, permeability of the aggregate, and occupancy fraction as defined in this paper. In certain limiting cases,  $\Omega$  converges to pre-existing analytical solutions for (i) an isolated impermeable sphere, (ii) an isolated uniformly porous sphere, (iii) an isolated composite sphere, (iv) a swarm of impermeable spheres, and (v) a swarm of uniformly porous spheres. This expression is then used to predict the specific resistance of aggregate cake formed on membrane surfaces.

© 2004 Elsevier B.V. All rights reserved.

**Keywords:** Fouling; Theory; Microfiltration; Fractal aggregate; Cell model

## 1. Introduction

Microfiltration (MF) and ultrafiltration (UF) are widely used to remove suspended solids, colloidal particles, macromolecules, bacteria, and viruses from suspensions as alternative, substitutional, or supplementary processes for conventional water and wastewater treatment. The major limiting factor of MF/UF use is the ratio of permeate flux (with appropriate water quality) to invested cost, since membrane fouling often gives rise to additional maintenance cost. While filtering particulate matter, MF/UF membranes undergo three different patterns of matter-stacking phenomena on their surfaces: concentration polarization, (followed by) colloidal cake/gel formation [1–16], and aggregate cake formation (i.e., a cake of retained aggregates composed of many small primary colloidal particles) [17–20]. Each pattern causes its own permeate flux decline behavior. Interestingly, particle aggregation occurring at relatively high ionic strength ( $\geq 0.01$  M) remarkably reduces the flux decline by developing on the membrane

surfaces a cake layer that is more porous than ones built with individual colloidal particles.

Waite et al. [17] observed distinctly different flux decline behaviors from aggregate cakes formed in different bulk phase aggregation schemes in stirred cell UF experiments. The work compared hydraulic resistances of cake layers comprised of aggregates formed by rapid aggregation and slow aggregation. Specific resistances of cake layers comprised of rapidly formed aggregates were at least one order of magnitude lower than cake layers comprised of slowly formed aggregates. The rapidly formed aggregates provide significantly less flux decline while showing very high overall porosity of more than 0.99 and fractal dimensions of 1.8–2.2 (which are between the typical fractal dimensions of diffusion-limited cluster aggregation (DLCA) of 1.75 [21] and diffusion-limited aggregation (DLA) of 2.5 [22]). On the other hand, the slowly formed aggregates cause more flux decline with a fractal dimension of 2.4, which is relatively higher than the typical value of reaction-limited cluster aggregation (RLCA) of 1.9–2.2 [23–28]. The differences in the fractal dimensions were attributed to one or more of the following: shear-induced aggregation, breakage, and reworking

\* Corresponding author. Tel.: +1 808 956 3718; fax: +1 808 956 5014.  
E-mail address: [albertsk@hawaii.edu](mailto:albertsk@hawaii.edu) (A.S. Kim).

(re-aggregation after breakage) mechanisms. In Waite et al.'s work, the aggregation regime was controlled by ionic strength (salt concentration), pH, and fulvic acid concentration, which affect aggregate structure, overall cake porosity, and flux decline behavior in a correlated manner. On the other hand, specific cake resistance was estimated by substituting the overall porosity of aggregates into the Carman–Kozeny equation [29], but its validity becomes questionable as the porosity increases above 0.8 (see Table 8-4.2 of Happel and Brenner [30]).

Using MF membranes in crossflow filtration mode, Hwang and Liu [20] investigated the effects of ionic strength (IS) on particle aggregation in bulk phase and the changes in (quasi-) steady-state permeate flux. They indicated that the steady-state permeate flux remained constant when  $IS < 0.01$  M, but quickly increased when  $IS > 0.01$  M because of the porous cake structure originated by the particle aggregation. Scrutinizing their experimental data, however, reveals that the permeate flux gradually decreases until the ionic strength reaches  $\sim 0.005$  M. This trend has also been seen in similar studies [12,31]. From Hwang and Liu's experiments, it can be therefore inferred that small aggregates can start forming near an ionic strength of 0.005 M, experiencing an interaction potential with no or low primary barrier. In theoretical aspects, they calculated the porosity profile across the entire cake layer consisting of aggregates as well as separated particles in void space outside the aggregates and then substituted the porosity value into the Carman–Kozeny equation to estimate cake resistance. This approach, as also found in Waite et al.'s work [17], implies possible replacement of a porous aggregate comprised of many primary particles by a single impermeable solid sphere that provides identical porosity and hydrodynamic drag. This method seems to be, however, less appropriate than replacing the aggregate by a uniformly porous sphere [32], which has an equal size and an equivalent volume-averaged permeability [33, 34].

The mechanism of aggregate cake collapse in terms of permeate flow velocity has been recently studied in Small Angle Neutron Scattering experiments by Cabane et al. [19]. They demarcated the dependence of scattering density  $I$  (of aggregates generated in rapid coagulation, i.e., diffusion-limited regime) on scattering vector  $q$  in three typical regions, where the inverse scattering vector  $q^{-1}$  is much less than, almost equal to, or much larger than the particle size. This method characterizes the structure of the bulk aggregates and aggregate-collapsed cake layers by their corresponding fractal dimensions, i.e., the slopes of  $\log I$  versus  $\log q$  plots. Without shear flow, the fractal dimension of bulk aggregates composed of spherical latex particles was found to be 2.45, which is somewhat higher than that of aggregates made in the RLCA regime. Furthermore, Cabane et al. investigated the collapsing criteria by increasing the trans-membrane pressure.

The results and implications of the recent research mentioned above indicate that the slow aggregation through

RLCA with or without ambient shear flow occurs at an ionic strength of an order of  $10^{-2}$  M, under which aggregation efficiency is very low, so that the generated aggregates are dense and compact with fractal dimensions typically greater than 2.0. As the ionic strength increases, the coagulation rate becomes fast, so that the formed aggregates show a sparse and loose structure with smaller fractal dimensions of usually less than 2.0. However, specific hydraulic resistance due to a swarm of aggregates, i.e., an aggregate cake, is still approximately determined in a qualitative as well as quantitative manner by simply substituting average aggregate porosity into hydrodynamic drag expressions for a swarm of impermeable solid spheres [17,20], e.g., the Carman–Kozeny equation [29] or possibly Happel's cell model [35]. Therefore, it is now of great necessity to accurately predict the permeate flux decline due to the cake layer formed with porous aggregates deposited on the membrane surfaces.

Extensive research has been conducted on creeping flow relative to porous spheres composed of mono-sized spheres. Happel [35] developed a hypothetical cell model to investigate the flow through a swarm of impermeable spheres packed in beds. His model converges to Stokes' equation for infinitely dilute colloidal suspensions. Brinkman [36] showed an expression of the flow through an isolated porous sphere of uniform permeability without detailed derivation. Later, Neale et al. [32] located the uniformly permeable sphere within Happel's hypothetical cell of a tangential stress-free surface, so that their expression reduces to Happel's if permeability of the porous sphere vanished. Masliyah and Neale [37] developed a mathematical expression that includes Stokes' equation and Brinkman's [36] equation by considering an isolated composite sphere comprised of a solid core and a porous shell. They used their derived expression to investigate the settling velocity of a solid sphere, to which various flexible threads are attached. Besides the analytic expressions [32,35–37] mentioned above, Ooms et al. [38] numerically confirmed Brinkman's equation [36] that was reported without derivations. Moreover, Veerapaneni and Wiesner [33] investigated the hydrodynamic properties of an isolated fractal aggregate with radially varying porosity and hence permeability by considering many consecutive thin shells of different constant permeabilities.

From a hydrodynamic point of view, the flow through a uniform porous sphere can be categorized into two representative types: a slow interior flow driven by fluid pressure and a fast exterior flow due to shear stress around the permeable sphere surface [39]. This phenomenon is more apparent in a fractal aggregate whose central region is much denser than its edge. Therefore, in our work, a fractal aggregate characterized by its length scale (radius) and fractal dimension (followed by radially varying local permeability) is simplified by an inner spherical core of impermeable solidity and an outer porous shell of uniform permeability. Following Neale et al.'s [32] approach, we position the simplified aggregate at the center of the tangential stress-free

cell [35], apply proper boundary conditions, and calculate the hydrodynamic drag due to a swarm of the simplified aggregates.

## 2. Theoretical

### 2.1. Flow through a swarm of aggregates

A primary assumption used in this study is that a solid spherical core surrounded by a porous shell (as shown in Fig. 1) is hydrodynamically equivalent to a fractal aggregate with radially varying permeability. The radius of the impermeable core, the distance between the center of the core and the outer surface of the shell (i.e., aggregate radius), and the radius of the hypothetical spherical cell (on which the tangential stress vanishes [35]) are denoted as  $a$ ,  $b$  ( $>a$ ) and  $c$  ( $>b$ ), respectively. Therefore,  $b - a$  is the thickness of the shell characterized by its constituent primary particles of radius  $a_p$ , porosity  $\varepsilon$ , and thereby accompanying permeability  $\kappa$ . Relative to this composite sphere (i.e., a core with a shell) in the hypothetical cell, the creeping flow of Newtonian fluid with absolute viscosity  $\mu$  is considered to be steady and axisymmetric. For mathematical convenience, the center of the composite sphere is selected as the origin of the spherical coordinates  $[r, \theta, \varphi]$ , while the fluid is partially passing through the composite sphere and approaching the membrane surface in the  $-z$  direction at velocity  $V$ .

#### 2.1.1. Governing equations

The governing equations of incompressible Newtonian creeping flow in void space are

$$\mu \nabla^2 u = \nabla p \quad (1)$$

and

$$\nabla \cdot u = 0 \quad (2)$$

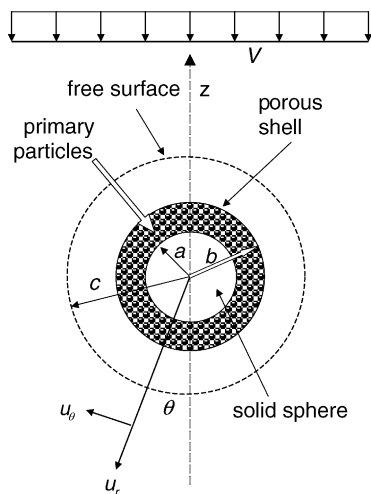


Fig. 1. Cell model of tangential stress-free surface applied to an impermeable solid sphere with a porous shell consisting of primary particles of radius  $a_p$ .

where  $u = [u_r, u_\theta, u_\varphi]$  denotes the fluid velocity vector and  $p$  is the fluid pressure. The corresponding equation for describing Newtonian creeping flow through uniformly porous medium of permeability  $\kappa$  is known as Brinkman's equation (Brinkman's extension of Darcy's law), i.e.,

$$\mu^* \nabla^2 u^* - \frac{\mu^*}{\kappa} u^* = \nabla p^* \quad (3)$$

with the macroscopic incompressibility assumption [40,41] of

$$\nabla \cdot u^* = 0 \quad (4)$$

where  $*$  denotes any macroscopically averaged quantity specifically pertaining to the porous medium. In this light,  $\mu^*$  represents an effective viscosity in the porous medium, often assumed identical to  $\mu$ , especially when the porosity of the medium is high and hence very permeable. Therefore, Eqs. (1) and (3) are valid within the void space ( $b \leq r \leq c$ ) and the porous shell ( $a \leq r \leq b$ ), respectively, with the incompressibility of the fluid maintained in both void space and porous medium (Eqs. (2) and (4)). Analytical expressions of permeability  $\kappa$  as a function of solid volume fraction  $\phi (=1 - \varepsilon)$  and primary particle radius  $a_p$  can be found elsewhere [34].

#### 2.1.2. Boundary conditions

The boundary conditions, which are physically realistic and mathematically consistent for the current problem, are as follows:

$$u_r^*(a, \theta) = 0 \quad (5)$$

$$u_\theta^*(a, \theta) = 0 \quad (6)$$

$$u_r^*(b, \theta) = u_r(b, \theta) \quad (7)$$

$$u_\theta^*(b, \theta) = u_\theta(b, \theta) \quad (8)$$

$$\tau_{rr}^*(b, \theta) = \tau_{rr}(b, \theta) \quad (9)$$

$$\tau_{r\theta}^*(b, \theta) = \tau_{r\theta}(b, \theta) \quad (10)$$

$$u_r(c, \theta) = -V \cos \theta \quad (11)$$

$$\tau_{r\theta}(c, \theta) = 0 \quad (12)$$

with  $0 < \theta < 2\pi$ , where  $\tau_{rr}^{(*)}$  and  $\tau_{r\theta}^{(*)}$  denote the normal and tangential components of the stress tensor, respectively, i.e.,

$$\tau_{rr}^{(*)} = -p^{(*)} + 2\mu^{(*)} \frac{\partial u_r^{(*)}}{\partial r} \quad (13)$$

and

$$\tau_{r\theta}^{(*)} = \mu^{(*)} \left( \frac{1}{r} \frac{\partial u_r^{(*)}}{\partial r} + \frac{\partial u_\theta^{(*)}}{\partial r} - \frac{u_\theta^{(*)}}{r} \right) \quad (14)$$

No-slip boundary conditions are applied on the surface of the core sphere of radius  $a$  (Eqs. (5) and (6)). The normal and tangential components of velocity and stress tensor are considered to be continuous across the permeable interface at

$r = b$  (Eqs. (7)–(10)). The fluid velocity  $V$  exerted by the composite sphere is reflected in Eq. (11), which also corresponds to such a situation that the sphere moves in the opposite direction to velocity  $V$  where the fluid is stationary. The condition of a free tangential stress on the surface of the hypothetical cell, first used in Happel's original work [35], is implemented in Eq. (12) to mimic the adjacent presence of other aggregates of similar sizes. Additionally, it has been proven that the continuity of the normal stress (Eq. (9)) is equivalent to that of the fluid pressure [42,43], i.e.,

$$p^*(b, \theta) = p(b, \theta) \quad (15)$$

from the incompressibility of Eqs. (2) and (4).

### 2.1.3. Method of solutions

Independence of the flow on the azimuthal angle, so called cylindrical symmetry or axi-symmetry, introduces stream functions  $\psi$  and  $\psi^*$  related to the velocity fields by

$$u_r^* = \frac{-1}{r^2} \frac{\partial \psi^*}{\sin \theta \partial \theta} \quad (16)$$

and

$$u_\theta^* = \frac{1}{r \sin \theta} \frac{\partial \psi^*}{\partial r} \quad (17)$$

where  $0 < \theta < 2\pi$  for both outside (unstarred) and inside (starred) the shell. Taking the curl of Stokes' equation (Eq. (1)) and Brinkman's equation (Eq. (3)), one obtains

$$E^4 \psi = 0, \quad b \leq r \leq c \quad (18)$$

and

$$E^4 \psi^* - \kappa^{-1} E^2 \psi^* = 0, \quad a \leq r \leq b \quad (19)$$

respectively, where

$$E^2 = \frac{\partial^2}{\partial r^2} + \frac{\sin \theta}{r^2} \frac{\partial}{\partial \theta} \left( \frac{1}{\sin \theta} \frac{\partial}{\partial \theta} \right) \quad (20)$$

with the macroscopic assumption of

$$\frac{\mu}{\mu^*} = 1 \quad (21)$$

The respective general solutions of Eqs. (18) and (19) are

$$\psi(\xi, \theta) = \frac{\kappa V}{2} \left( \frac{A}{\xi} + B\xi + C\xi^2 + D\xi^4 \right) \sin^2 \theta, \quad \beta \leq \xi \leq \gamma \quad (22)$$

and

$$\psi^*(\xi, \theta) = \frac{\kappa V}{2} \left[ \frac{E}{\xi} + F\xi^2 + G \left( \frac{\cosh \xi}{\xi} - \sinh \xi \right) + H \left( \frac{\sinh \xi}{\xi} - \cosh \xi \right) \right] \sin^2 \theta, \quad \alpha \leq \xi \leq \beta \quad (23)$$

where  $\xi = r/\sqrt{\kappa}$ ,  $\alpha = a/\sqrt{\kappa}$ ,  $\beta = b/\sqrt{\kappa}$ , and  $\gamma = c/\sqrt{\kappa}$ . Satisfying the set of boundary conditions listed in Eqs. (5)–(12), the constants  $A, B, C, D, E, F, G$ , and  $H$  will have specific values, as given in Appendix A.

Integrating the normal and tangential stress distributions over the porous surface yields the drag force  $\mathbf{F}^1$  experienced by the composite sphere

$$\begin{aligned} \mathbf{F} &= 2\pi b^2 \int_0^\pi [\tau_{rr} \cos \theta - \tau_{r\theta} \sin \theta]_{r=b} \sin \theta d\theta \\ &= 6\pi\mu V b \Omega \end{aligned} \quad (24)$$

where

$$\Omega = + \frac{2B}{3\beta} \quad (25)$$

of which its physical meaning is

Hydrodynamic resistance experienced by a swarm of the composite spheres with a core of radius  $a$  and a porous shell of thickness  $b - a$

---

Hydrodynamic resistance experienced by an impermeable sphere of radius  $b$

The positive sign of Eq. (25) refers to the direction of the force (+z) that sustains the composite sphere in the downward ambient fluid flow toward the membrane surface.

### 2.1.4. Comparison with related works

The correctness of our expression of  $\Omega$  may be confirmed by scrutinizing five important cases for which analytical solutions are already available: (1) as  $\alpha \rightarrow \beta$  (or  $\kappa \rightarrow 0$ ) and  $\gamma \rightarrow \infty$ , Stokes' equation is obtained, i.e.,  $\Omega = 1$ , (2) as  $\alpha \rightarrow \beta$  (or  $\kappa \rightarrow 0$ ), Happel's well-known formula [35] is retrieved, i.e.,

$$\lim_{\alpha \rightarrow \beta} \Omega \equiv \Omega_H = \frac{1 + (2/3)\eta^5}{1 - (3/2)\eta + (3/2)\eta^5 - \eta^6} \quad (26)$$

where  $\eta^3 = b^3/c^3 (= \beta^3/\gamma^3)$  of which can be interpreted as the volume fraction of the sphere-packed porous medium, (3) as  $\alpha \rightarrow 0$  and  $\gamma \rightarrow \infty$ , Brinkman's equation [38,44] for an isolated homogeneously permeable sphere of radius  $b$  is replicated, i.e.,

$$\lim_{\substack{\alpha \rightarrow 0 \\ \gamma \rightarrow \infty}} \Omega \equiv \Omega_B = \frac{2\beta^2(1 - \tanh \beta/\beta)}{2\beta^2 + 3(1 - \tanh \beta/\beta)}, \quad (27)$$

(4) as  $\alpha \rightarrow 0$ , Eq. (25) in this study becomes Eq. (30) of Neale et al.'s work [32], i.e.,

---

<sup>1</sup> The necessary FORTRAN subroutine to calculate  $\mathbf{F}$  can be provided upon request to the corresponding author.

$$\begin{aligned} \lim_{\alpha \rightarrow 0} \Omega &\equiv \Omega_{\text{NEN}} \\ &= \frac{2\beta^2 + (4/3)\beta^2\eta^5 + 20\eta^5}{2\beta^2 - 3\beta^2\eta + 3\beta^2\eta^5 - 2\beta^2\eta^6 + 90\beta^{-2}\eta^5 + 42\eta^5} \\ &\quad - \frac{(\tanh \beta/\beta)(2\beta^2 + 8\beta^2\eta^5 + 20\eta^5)}{-30\eta^6 + 3 - (\tanh \beta/\beta)(-3\beta^2\eta + 15\beta^2\eta^5} \\ &\quad - 12\beta^2\eta^6 + 90\beta^{-2}\eta^5 + 72\eta^5 - 30\eta^6 + 3) \end{aligned} \quad (28)$$

and finally (5) as  $\gamma \rightarrow \infty$ , Masliyah and Neale's work [37] is reproduced, but the detailed formula of  $\lim_{\gamma \rightarrow \infty} \Omega$  is omitted in this paper due to the length and complexity of their analytic expression. Proving the above five known expressions by inspecting certain limiting cases of  $\Omega$ , we confirm that our general solution of Eq. (25) is mathematically correct with appropriate physical meanings.

## 2.2. Filtration equation: Darcy's law

Permeate flux across a membrane containing a deposited layer (i.e., aggregate cake layer in this study) may be described by Darcy's law with the resistance-in-series model:

$$V = \frac{\Delta P}{\mu(R_m + R_c)} \quad (29)$$

where  $V$  is the permeate velocity,  $\Delta P$  the pressure drop across the membrane,  $R_m$  the membrane resistance, and  $R_c$  the cake resistance, which can be described as

$$R_c = r_c \delta_c \quad (30)$$

where  $r_c$  and  $\delta_c$  are the specific resistance and thickness of the cake layer, respectively. In this model of the system shown in Fig. 1, the pressure gradient across the cake layer should be equal in magnitude to the drag force density inside the hypothetical cell, of which the radius is  $c$ , i.e.,

$$\frac{\Delta P_c}{\delta_c} = \frac{6\pi\mu b V \Omega(\alpha, \beta, \gamma)}{4\pi c^3/3} \quad (31)$$

where  $\Delta P_c = \Delta P - \mu R_m V$ . Manipulating Eq. (31) with Eqs. (29) and (30) gives

$$r_c = \frac{\Omega(\alpha, \beta, \gamma)}{2b^2/9\lambda} \quad (32)$$

where  $\lambda = \eta^3$  is defined in this study as "occupancy fraction", which is always greater than the volume fraction  $\phi$  of the aggregate cake layer due to the porous region (i.e.,  $a < r < b$ ) of the composite sphere. It is worth noting that the term  $2b^2/9\lambda$  in Eq. (32) is the permeability of solid spheres of radius  $b$  in a dilute limit, while the porous shell is disappearing (i.e.,  $\lambda \rightarrow \phi$ ). For the case of a swarm of solid spheres, the corresponding  $b^2 r_c$  is then obtained by substituting Happel's cell

model (Eq. (26)) into Eq. (32), i.e.,

$$b^2 r_{c,H} = \left( \frac{9\phi}{2} \right) \left( \frac{1 + (2/3)\phi^{5/3}}{1 - (3/2)\phi^{1/3} + (3/2)\phi^{5/3} - \phi^2} \right) \quad (33)$$

or often by Carman–Kozeny equation instead

$$b^2 r_{c,CK} = \left( \frac{9\phi}{2} \right) \Omega_{CK} \quad (34)$$

where

$$\Omega_{CK} = \frac{2k\phi}{(1 - \phi)^3} \quad (35)$$

with empirically found  $k \approx 5$ . The dimensionless specific cake resistance  $b^2 r_c$  of Eq. (33) or (34) is commonly used to estimate the resistance  $R_c$  with the volume fraction of the colloidal cake layer [9,12,45–47], so they will be compared to  $b^2 r_c$  of the aggregate cake layer in the following section.

## 3. Results and discussion

### 3.1. Dimensionless specific cake resistance, $b^2 r_c$

Fig. 2 shows the dimensionless specific cake resistance  $b^2 r_c$  defined in Eq. (32) as a function of the occupancy fraction  $\lambda$  with  $\alpha$  and  $\beta$  ( $>\alpha$ ) and  $\gamma$  ( $=\beta/\sqrt[3]{\lambda}$ ) values, and it also illustrates  $b^2 r_{c,H}$  and  $b^2 r_{c,CK}$ , which are defined in Eqs. (33) and (34), respectively. The corresponding analysis of Fig. 2 follows.

#### 3.1.1. Converging to Happel's cell model

Figs. 2(a)–(c) show that  $b^2 r_c$  reaches  $b^2 r_{c,H}$  (also shown in Fig. 2(d)), when the porous shell disappears, i.e.,  $\alpha \rightarrow \beta$  (so consequently  $\lambda \rightarrow \phi$ ). This is already analytically proven in Eq. (26).

#### 3.1.2. An aggregate as a uniform porous sphere

On the other hand,  $b^2 r_c$  with  $\alpha = 0$  declines with decreasing  $\beta$  ( $\equiv b/\sqrt{\kappa}$ ) from increasing constant permeability  $\kappa$ . The composite sphere becomes a uniformly porous sphere of radius  $b$  in this case. If both  $\alpha$  and  $\beta$  ( $\geq \alpha$ ) reach zero, then  $b^2 r_c$  vanishes accordingly since no material is physically retained on the membrane surface.

#### 3.1.3. Effect of porous shell thickness

Comparing  $b^2 r_c(\alpha, \beta, \gamma)$  of  $\alpha = \beta$  with  $\alpha = 0.95\beta$ , where  $\lambda = 0.5$ , gives a quite interesting result: the thin porous shell, of which thickness is only 5% of the aggregate radius  $b$ , significantly reduces  $b^2 r_c$  down to 60% compared to  $b^2 r_c(\beta, \beta, \gamma)$ . This result indicates that even dense aggregates (generated in slow aggregation regime) provide significantly less drag compared to solid spheres of the same size, and it further implies that a cake layer composed of relatively big colloidal particles with only small roughness can drastically

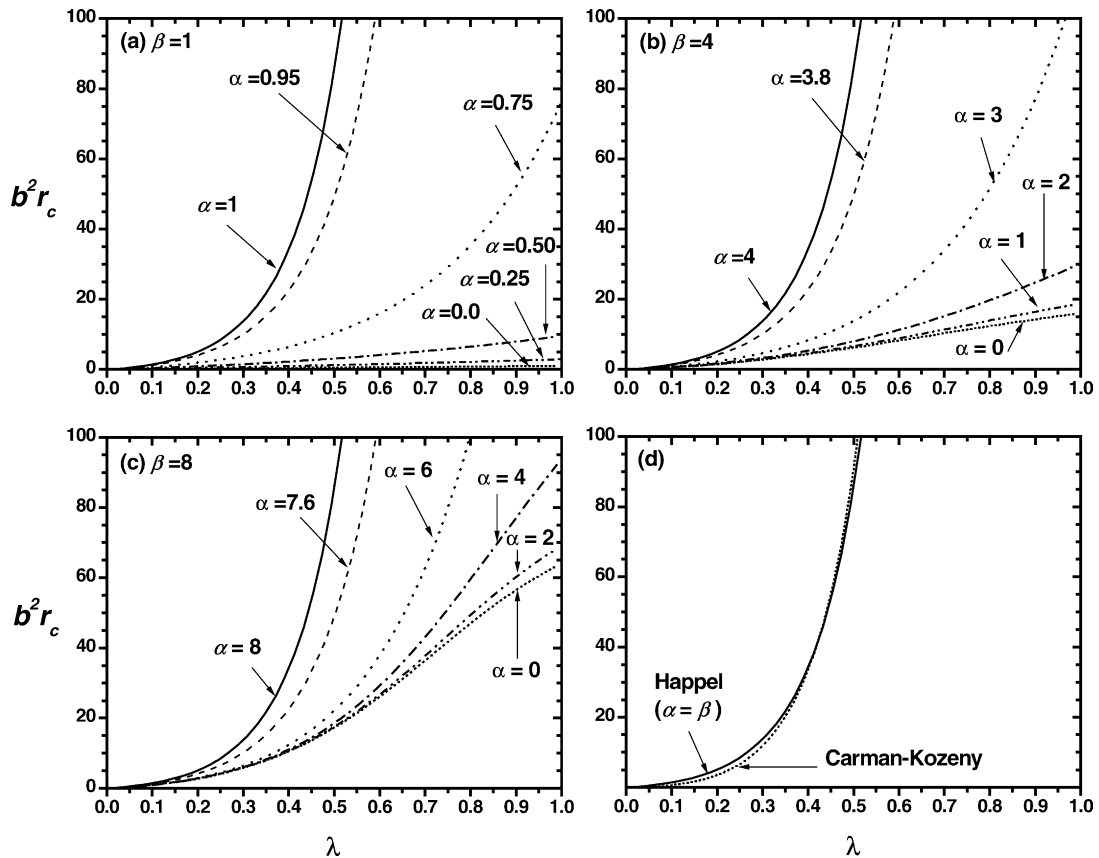


Fig. 2. Dimensionless specific cake resistance  $b^2 r_c(\alpha, \beta, \gamma)$  as a function of the occupancy fraction  $\lambda$ : (a)  $\beta = 1$ , (b)  $\beta = 4$ , and (c)  $\beta = 8$ , and (d) Happel (Eq. (33)) and Carman–Kozeny (Eq. (34)) expressions. For each case of (a)–(c),  $\alpha$  values are 0.95, 0.75, 0.50, 0.25, and 0.0 of each  $\beta$ , and  $\gamma = \beta/\sqrt[3]{\lambda}$ .

reduce the cake resistance, avoiding no-slip boundary conditions on outer surfaces of the rough particles.

### 3.1.4. Effect of overlap and/or breakage

Another interesting behavior of  $b^2 r_c$  in Figs. 2(a)–(c) is that, unlike Eqs. (33) and (34),  $b^2 r_c$  does not diverge as long as  $\alpha$  is less than (but not equal to)  $\beta$ , even if the occupancy fraction  $\lambda$  reaches unity. Table 1 shows the values of  $b^2 r_c$ , used in Fig. 2, with  $\alpha$  and  $\beta$ , where  $\lambda = 1$ . Apparently,  $b^2 r_c$  with  $\alpha = 0.95\beta$  is significantly larger than that of  $\alpha = 0$ , but it does remain finite because the fluid flow still can penetrate the remaining porous region,  $\alpha < \xi < \beta$  ( $=\gamma$ ), equivalently  $a < r < b$  ( $=c$ ).

The limit of  $\lambda \rightarrow 1$  corresponds to the following cases. First, the aggregates are closely packed, so that portions of their sparse edges are somehow overlapped and thus partially broken to a certain extent. Individual or small groups of primary particles detached from the aggregates can be re-agglomerated with themselves or re-attached to a nearby aggregate. Then, the original void spaces among the unbroken aggregates can be filled with the re-organized primary particles. Second, when the cake layer is composed of relatively big colloidal particles on which long polymer chains are adsorbed, particle-interconnection oriented by the polymer chains generates a fibrous porous medium among the colloidal particles, filling the void spaces. The limiting value

of  $b^2 r_c$  with  $\lambda = 1$  decreases when  $\alpha$  and/or  $\beta$  decreases: lower volume fraction of the porous shell provides higher permeability  $\kappa$ , so smaller values of both  $\alpha$  and  $\beta$ , but smaller radius of the solid core reduces only  $\alpha$ .

Table 1  
The value of  $b^2 r_c$  with  $\lambda = 1$

$\beta$	$\alpha$	$b^2 r_c$
1	1.00	$\infty$
1	0.95	$1.119 \times 10^4$
1	0.75	$7.632 \times 10^1$
1	0.50	$9.563 \times 10^0$
1	0.25	$2.875 \times 10^0$
1	0.00	$1.000 \times 10^0$
4	4.00	$\infty$
4	3.80	$1.138 \times 10^4$
4	3.00	$1.141 \times 10^2$
4	2.00	$3.017 \times 10^1$
4	1.00	$1.885 \times 10^1$
4	0.00	$1.600 \times 10^1$
8	8.00	$\infty$
8	7.60	$1.196 \times 10^4$
8	6.00	$2.328 \times 10^2$
8	4.00	$9.375 \times 10^1$
8	2.00	$6.911 \times 10^1$
8	0.00	$6.400 \times 10^1$

Note: Numerical value of  $b^2 r_c$  plotted in Fig. 2 with  $\lambda = 1$  are listed here. The values of  $\alpha$  and  $\beta$  are same as used in Fig. 2.

### 3.2. Happel's cell model and Carman–Kozeny equation

#### 3.2.1. Invalidity of Carman–Kozeny equation for highly porous aggregates

As shown in Fig. 2(d), the Happel (Eq. (33)) and Carman–Kozeny (Eq. (34)) equations are almost indistinguishable. However, if permeability as inverse of  $r_c$  is considered, the Carman–Kozeny equation shows a quite different asymptotic behavior from Happel's expression in an infinitely dilute limit. For solid spheres of radius  $b$  in the dilute limit, Stokes' equation brings out  $\Omega = 1$  and leaves the corresponding permeability as  $2b^2/9\phi$ . In this circumstance, Eq. (35) becomes

$$\lim_{\phi \rightarrow 0} \Omega_{c,CK} \approx 2k\phi \quad (36)$$

which implies the invalidity of the Carman–Kozeny equation where  $\phi \leq 0.1$ , bolstering the necessary condition to use Eq. (34), i.e.,  $\phi \geq 0.3$  with  $k \approx 5$  (see Table 8-4.2 of Happel and Brenner [30]). Therefore, it is quite apparent that the Carman–Kozeny equation highly underestimates the dimensionless drag force  $\Omega$  and thereby significantly overestimates the corresponding permeability of highly porous aggregates (see Fig. 1 of Kim and Stolzenbach [34]) that are often found in natural and engineered systems [48–52].

#### 3.2.2. Equivalent solid sphere

Some researchers replaced the fractal aggregate by an equivalent, but smaller, solid sphere and applied the Carman–Kozeny equation to estimate the cake resistance [17,20]. Although Waite et al. [17] calculated quite reasonable values of cake porosity by considering several cases of fractal dimension and ratios of aggregate to primary particle size (i.e.,  $b/a_p$ ), the estimation of the specific cake resistance<sup>2</sup> through

$$\frac{9k(1 - \varepsilon)}{\rho_p a_p^2 \varepsilon^3} \quad (37)$$

where  $\rho_p$  is the mass density of the primary particles, can be underestimated due to the coefficient  $k$ . This accounts for why the value of  $k$  is actually about 10 times greater than the empirically obtained value of 5.0, if the porosity reaches 0.99 (see Table 3 of Waite et al. [17] and Table 8-4.2 of Happel and Brenner [30]). On the other hand, Hwang and Liu [20] used a porosity-dependent  $k$  for flow perpendicular to the cylinders (Eq. (8-4.33) of Happel and Brenner [30]) to evaluate the specific cake resistance defined as Eq. (37). It seems, however, more reasonable to use  $k$  for flow through random orientation of cylinders. They used a different interpretation of Happel's original cell model [35] by considering additional void spaces among the hypothetical cells of free tangential stress [53]. Nevertheless, the measured and estimated porosity at high ionic strength ( $\geq 0.01$  M), i.e., fast aggregation regime,

are within the range of 0.67–0.73, although faster axial velocity seems to affect the structure of aggregates or partially break the aggregates to a certain extent.

An alternative way of linking the porosity and the specific cake resistance of an aggregate is to treat the aggregate as a uniform porous sphere [36], if the porosity is close to 1.0. For a relatively smaller or denser aggregate generated in a slow aggregation regime, however, negligible flow near the central region of the aggregate should be implemented by possibly locating a solid core at the center of the uniform porous sphere. This is to pragmatically consider deflecting flow around the edge of the aggregate [34,39] and thereby approximately estimate the specific cake resistance defined in Eq. (32). In this light, the constant permeability  $\kappa$  of the porous shell and the solid core radius  $a$  should be obtained by the fractal nature of the aggregate (see next section).

### 3.3. Gauging $\alpha$ , $\beta$ , and $\gamma$

The three parameters,  $\alpha$ ,  $\beta$ , and  $\gamma$  can be estimated in the following way. For simplicity, an isolated aggregate comprised of many primary particles of radius  $a_p$  is considered to estimate  $\alpha$  and  $\beta$ . The aggregate is characterized by fractal dimension  $D_f$  and radius  $b$ , and then it is mapped into an isolated composite sphere (i.e.,  $\gamma \rightarrow \infty$ ) of the same size. The aggregate and the composite spheres are considered to have identical average volume fractions and gyration radii.

#### 3.3.1. A realistic aggregate

The local volume fraction profile  $\phi(r)$  at a distance  $r$  from the center of the aggregate can be represented as

$$\phi(r) = \phi_0 \left( \frac{r}{a_p} \right)^{D_f - 3}, \quad 0 < r < b \quad (38)$$

where  $\phi_0$  is a proportionality constant. The average volume fraction of the aggregate, defined as volume occupied by the primary particles over total volume of the aggregate, can be calculated as

$$\langle \phi \rangle = \frac{\int_0^b \phi(r) 4\pi r^2 dr}{(4\pi/3)b^3} = \frac{3\phi_0}{D_f} \left( \frac{b}{a_p} \right)^{D_f - 3} \quad (39)$$

The gyration radius  $R_g$  of the aggregate is estimated using the local volume fraction profile of Eq. (38) [54,55]

$$R_g^2 = \frac{\int_0^b r^2 \phi(r) 4\pi r^2 dr}{\int_0^b \phi(r) 4\pi r^2 dr} = b^2 \frac{D_f}{D_f + 2} \quad (40)$$

or

$$R_g = b \sqrt{\frac{D_f}{D_f + 2}} \quad (41)$$

The hydrodynamic radius of the aggregate is defined as

$$R_h = \frac{F}{6\pi\mu V} \quad (42)$$

<sup>2</sup> The specific cake resistance of Waite et al.'s work [17] is defined as cake resistance divided by deposited mass per unit membrane area.

The total number of primary particles within the aggregate is related to the fractal dimension and radius of the aggregate, i.e.,

$$N = \frac{\int_0^b \phi(r) 4\pi r^2 dr}{(4\pi/3)a_p^3} = \frac{3\phi_0}{D_f} \left(\frac{b}{a_p}\right)^{D_f} \quad (43)$$

Sorensen and Roberts [56] used the following equation to link the number of primary particles  $N$  and the gyration radius of the aggregate  $R_g$

$$N = k_0 \left(\frac{R_g}{a_p}\right)^{D_f} \quad (44)$$

where  $k_0$  is, so-called, a prefactor varying with the fractal dimension. They generated many aggregates using computer simulation and estimated the prefactor of Eq. (44) by calculating the slope of  $\log N$  versus  $\log (R_g/a_p)$  plot. Substituting Eq. (41) into Eq. (44) gives

$$N = k_0 \left(\frac{D_f}{D_f + 2}\right)^{D_f/2} \left(\frac{b}{a_p}\right)^{D_f} \quad (45)$$

and equating Eqs. (43) and (45) provides

$$\phi_0 = k_0 \frac{D_f}{3} \left(\frac{D_f}{D_f + 2}\right)^{D_f/2} \quad (46)$$

Therefore, the proportionality constant  $\phi_0$  of Eq. (38) can be determined by the fractal dimension  $D_f$  and the prefactor  $k_0$  in Eq. (46).

### 3.3.2. A composite sphere

The local volume fraction profile  $\phi_{cs}(r)$  of a composite sphere can be bisected into two regions of constant volume fraction

$$\phi_{cs}(r) = \begin{cases} 1 & 0 < r < a \\ \phi_{sh} & a < r < b \end{cases} \quad (47)$$

where  $\phi_{sh}$  is volume fraction of the porous shell. The average volume fraction of the composite sphere is then

$$\langle \phi \rangle = \frac{\int_0^b \phi_{cs}(r) 4\pi r^2 dr}{(4\pi/3)b^3} = \hat{a}^3 + \phi_{sh}(1 - \hat{a}^3) \quad (48)$$

where  $\hat{a} = a/b$ . The gyration radius of the composite sphere, calculated by the same definition of Eq. (40), is

$$R_g^2 = \frac{\int_0^b r^2 \phi_{cs}(r) 4\pi r^2 dr}{\int_0^b \phi_{cs}(r) 4\pi r^2 dr} = b^2 \frac{3(\hat{a}^5 + \phi_{sh}(1 - \hat{a}^5))}{5(\hat{a}^3 + \phi_{sh}(1 - \hat{a}^3))} \quad (49)$$

From Eq. (42), the hydrodynamic radius of the composite sphere is then simply

$$R_h = b\Omega \quad (50)$$

### 3.3.3. Equivalence between the aggregate and the composite sphere

The realistic aggregates can be mapped into the composite sphere by equating Eqs. (39) and (48) and Eqs. (40) and

(49). Then, the shell volume fraction  $\phi_{sh}$  and the dimensionless core radius  $\hat{a}$  ( $=a/b$ ) can be simultaneously obtained. In this case an expression of permeability  $\kappa$  should be selected to estimate  $\alpha$  and  $\beta$ . Because most fractal aggregates have a tree-like, branched local structure, Davies' permeability expression [57] for fibrous porous media is suitable for this study

$$\kappa_D = \frac{a_p^2}{16\phi^{1.5}(1 + 56\phi^3)} \quad (51)$$

Therefore, the calculated shell volume fraction  $\phi_{sh}$  is used to estimate the shell permeability in a dimensionless form,  $\kappa_{sh}/a_p^2 = \kappa_D(\phi_{sh})/a_p^2$ . From fractal dimension  $D_f$  and aggregate radius  $b$ ,  $\alpha$  and  $\beta$  can be then calculated as

$$\beta = \frac{b/a_p}{\sqrt{\kappa_{sh}/a_p^2}} \quad (52)$$

and

$$\alpha = \frac{a/a_p}{\sqrt{\kappa_{sh}/a_p^2}} = \hat{a}\beta \quad (53)$$

### 3.3.4. Verification of the mapping approach

Chen et al. [58] reported that the ratio of the hydrodynamic radius  $R_h$  to the gyration radius  $R_g$  is 0.875 using 133 DLCA aggregates. Their aggregates are composed of 50–350 primary particles with an average fractal dimension of 1.78. Sorensen and Roberts [56] performed similar computer simulations and found that their DLCA aggregates have the same fractal dimension of 1.78 and the corresponding prefactor  $k_0$  of 1.27. So, we used  $D = 1.78$  and  $k_0 = 1.27$  and estimated the ratio of  $R_h/R_g$  with the number of primary particles  $N$  from 50 to 350 at intervals of 50. The ratio of  $b/a_p$  in Eq. (52) is estimated by the number of primary particles with Eq. (45). As shown in Table 2, the average value of  $R_h/R_g$  obtained by our mapping method with the seven different values of  $N$  is  $0.910 \pm 0.015$ . Relative errors are within 6% in magnitude in comparison with Chen et al.'s result. Therefore, we are confident that this mapping method of a fractal aggregate into a composite sphere is valid from both hydrodynamic and geometrical stand points.

### 3.3.5. Occupancy ratio $\lambda$

The volume fraction of the cake layer, which is comprised of non-interacting mono-dispersed spherical particles (i.e., identical hard spheres), is typically assumed as having random loosely packing ratio, 0.60, or random loosely packing ratio, 0.64 [59–61]. A slow aggregation regime renders dense and compact aggregates, while a fast aggregation regime provides sparse and loose aggregates. However, both types of aggregates commonly have a tree-like edge structure that allows overlap to a certain extent among adjacent aggregates in contact. Therefore, the occupancy ratio  $\lambda$  would be greater

Table 2  
Properties of composite spheres modeled by the mapping approach with  $D = 1.78$  and  $k_0 = 1.27$

$N$	$\phi_0$	$\langle \phi \rangle$	$\phi_{sh}$	$\hat{a}$	$a/a_p$	$b/a_p$	$\kappa_D(\phi_{sh})/a_p^2$	$\alpha$	$\beta$	$R_h$	$R_g$	$R_h/R_g$
50	0.38549	0.03310	0.02569	0.19665	2.256	11.474	15.160	0.5795	2.9468	6.9690	7.873	0.88518
100	0.38549	0.02059	0.01603	0.16667	2.823	16.936	30.790	0.5087	3.0522	10.4460	11.622	0.89886
150	0.38549	0.01559	0.01216	0.15148	3.222	21.269	46.621	0.4718	3.1149	13.2450	14.595	0.90748
200	0.38549	0.01280	0.00999	0.14160	3.540	25.000	62.590	0.4474	3.1599	15.6760	17.155	0.91376
250	0.38549	0.01099	0.00858	0.13440	3.809	28.338	78.664	0.4294	3.1951	17.8660	19.446	0.91871
300	0.38549	0.00969	0.00757	0.12881	4.044	31.395	94.823	0.4153	3.2241	19.8800	21.544	0.92279
350	0.38549	0.00872	0.00682	0.12428	4.255	34.235	111.053	0.4037	3.2487	21.7600	23.493	0.92626

Note: The average value of  $R_h/R_g$  in this table is  $0.910 \pm 0.015$ . The proportionality constant  $\phi_0$  is kept unchanged since it is determined with only  $D_f$  and  $k_0$ . Other quantities are calculated based on definitions in Section 3.3. The small values of  $\hat{a}$  and  $\phi_{sh}$  reflect sparse edge structure of the DLCA aggregates.

than or at least equal to the random packing ratio of identical hard spheres, but apparently depends on fractal dimension of aggregates. To estimate more realistic value of  $\lambda$ , it is necessary to conduct micro-hydrodynamics-level simulations, and the results should be verified with a set of experiments.

### 3.4. Interpretation of settling velocity

As a reverse concept of hydrodynamic drag force, settling velocity of spherical objects can be addressed easily by analyzing  $\Omega$  defined in Eq. (25), of which its inverse is interpreted as

$$\Omega^{-1}(\alpha, \beta, \gamma)$$

$$\frac{\text{Settling velocity of a swarm of the composite spheres with a core of radius } a \text{ and a porous shell of thickness } b - a}{\text{Settling velocity of an impermeable sphere of radius } b} \quad (54)$$

where the composite and impermeable spheres have the same mass within the common radius  $b$ . For a single isolated composite sphere (i.e.,  $\gamma \rightarrow \infty$ ), Eq. (54) represents the settling velocity ratio of the composite sphere to that of a solid sphere of the same size, which is denoted here as  $\Omega_\infty^{-1} = \Omega^{-1}(\alpha, \beta, \gamma \rightarrow \infty)$ . Then, the ratio of  $\Omega^{-1}$  to  $\Omega_\infty^{-1}$  provides the dimensionless settling velocity defined as

$$v_s \equiv \frac{\Omega^{-1}}{\Omega_\infty^{-1}} = \frac{\Omega(\alpha, \beta, \gamma \rightarrow \infty)}{\Omega(\alpha, \beta, \gamma)} \quad (55)$$

The physical meaning of Eq. (55) is

$$\frac{\text{Settling velocity of a swarm of composite spheres}}{\text{Settling velocity of an isolated composite sphere}}$$

Therefore,  $v_s$  of a swarm of solid spheres and uniformly porous spheres can be assessed by taking limits of  $\alpha \rightarrow \beta$  [35] and  $\alpha \rightarrow 0$  [32], respectively.

Fig. 3 shows the dimensionless settling velocity  $v_s$  defined in Eq. (55) as a function of the occupancy fraction  $\lambda$  with the two  $\beta$  values of 1 and 8, where  $0 \leq \alpha \leq \beta$  and  $\gamma = \beta/\sqrt[3]{\lambda}$ . The corresponding analyses are as follows: (1) similar to the explanation for Fig. 2, the dimensionless settling velocities for

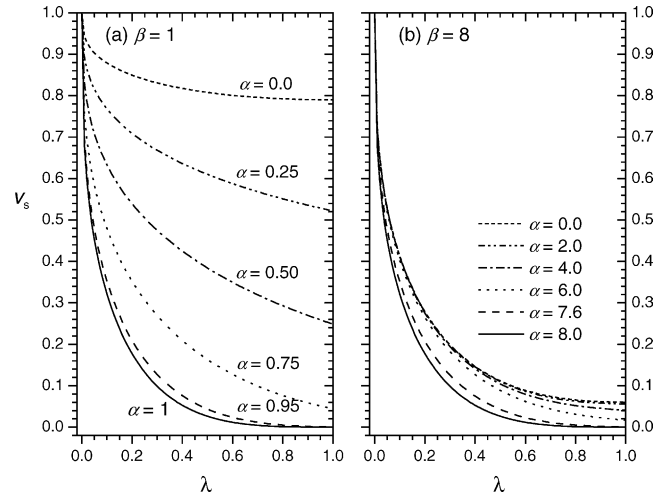


Fig. 3. Dimensionless settling velocity as a function of occupancy fraction  $\lambda$ : (a)  $\beta = 1$ , and (b)  $\beta = 8$ . For each case,  $\alpha$  values are 0.95, 0.75, 0.50, 0.25, and 0.0 of each  $\beta$ , and  $\gamma = \beta/\sqrt[3]{\lambda}$ .

solid spheres (i.e.,  $\alpha = \beta$ ) are identical in Fig. 3 with different  $\beta$  values; (2) as  $\alpha$  decreases,  $v_s$  increases at a fixed value of  $\lambda$  because the solid core shrinks accordingly and leaves less surface area of non-slip fluid flow; (3) interestingly, unlike the specific cake resistance  $b^2 r_c$  shown in Fig. 2, the difference between settling velocities of solid spheres ( $\alpha = \beta$ ) and that of rough spheres ( $\alpha = 0.95\beta$ ) is not remarkable as illustrated in Fig. 3; and (4) for relatively large  $\beta$  due to small permeability of the porous shell, the presence of the solid core does not significantly affect the settling velocity because the flow penetration into the composite sphere is negligible. Additionally it is worth noting that quantitative comparison of any two curves in Fig. 3(a) and (b) with a same  $\alpha$  (except  $\alpha = \beta$ ) may not provide appropriate physical meaning since the reference velocities (i.e.,  $\Omega_\infty^{-1}$ ) are not identical due to the different  $\beta$  values.

## 4. Concluding remarks

The specific resistance of an aggregate cake was investigated by developing a simple hydrodynamic model in which a fractal aggregate, typically characterized by radially

decreasing mass density with power law, was replaced by a hydrodynamically and geometrically equivalent composite sphere that is comprised of a solid core and a porous shell and located in the center of Happel's hypothetical cell. The equivalent sphere provides a general expression of dimensionless drag force  $\Omega$ , including Stokes' equation and other four pre-developed equations [32,35–37]. This simple model is then able to quantify the specific resistances of the cake layer composed of similar-sized aggregates, possibly characterized by representative permeability and size of central core of zero porosity. Even if aggregates generated in a slow aggregation regime have a relatively small and dense structure with the fractal dimension typically more than 2.0, their permeable edges can drastically reduce hydrodynamic resistance compared to solid spherical particles of the same size. Additionally, the presented solution is applied to estimate hindered settling velocity of fractal aggregates and/or polymer-adsorbed big colloidal particles.

### Acknowledgements

The authors acknowledge support for the research activities from the Department of the Interior, U.S. Geological Survey (grant no. 01HQFR0079), through the Hawaii Water Resources Research Center, as well as from the University Research Council at the University of Hawaii at Manoa, Honolulu. This is contributed paper CP-2004-09 of the Water Resources Research Center.

### Appendix A

Detailed expressions of coefficients  $A$  through  $H$  of the stream functions (Eqs. (22) and (23)), satisfying the boundary conditions of Eqs. (5)–(12), are prescribed below

$$D = \frac{D_{11}\gamma}{-2J\gamma^6 + D_{05}\gamma^5 + D_{01}\gamma + D_{00}} \quad (\text{A.1})$$

where

$$J = 3(\alpha^2 - 1) \sinh \Delta + (3\alpha + 2\beta^3 + 3\beta + \alpha^3) \cosh \Delta - 6\alpha \quad (\text{A.2})$$

$$D_{11} = -6\alpha\beta^3 + \beta^2(2\beta^4 + 12\beta^2 + 3\alpha\beta + \alpha^3\beta - 9\alpha^2) \cosh \Delta - 3\beta^2(2\beta^3 - \alpha^2\beta + 4\beta + 3\alpha + \alpha^3) \times \sinh \Delta \quad (\text{A.3})$$

$$D_{05} = 3(-3\alpha^2 + 2\beta^4 + \alpha^3\beta + 3\alpha\beta) \cosh \Delta + 3(3\alpha^2\beta - 3\alpha - 2\beta^3 - \alpha^3) \sinh \Delta \quad (\text{A.4})$$

$$D_{01} = -3\beta^3(3\alpha\beta^2 + 2\beta^5 + 28\beta^3 + 60\alpha + \alpha^3\beta^2 + 60\beta + 20\alpha^3 - 15\alpha^2\beta) \cosh \Delta + 3\beta^3(15\alpha\beta + 60 + 10\beta^4 + 48\beta^2 - 3\alpha^2\beta^2 + 5\alpha^3\beta - 60\alpha^2) \sinh \Delta + 36\alpha\beta^3(10 + 3\beta^2) \quad (\text{A.5})$$

$$D_{00} = 2\beta^3(3\alpha\beta^3 + 2\beta^6 - 18\alpha^2\beta^2 + 30\beta^4 + \alpha^3\beta^3 + 45\alpha^3\beta + 135\alpha\beta - 135\alpha^2) \cosh \Delta - 6\beta^3(45\alpha + 6\alpha\beta^2 + 4\beta^5 + 10\beta^3 + 2\alpha^3\beta^2 - 45\alpha^2\beta - \alpha^2\beta^3 + 15\alpha^3) \sinh \Delta - 120\alpha\beta^6 \quad (\text{A.6})$$

and

$$\Delta = \beta - \alpha \quad (\text{A.7})$$

$$C = \frac{[-(4/3)J\gamma^5 + C_{12}\gamma^2 + C_{10}]D + (2/3)J\gamma^3}{(2/3)J\gamma^3 + C_{02}\gamma^2 + C_{00}} \quad (\text{A.8})$$

where

$$C_{12} = -5\beta^2(2\beta^3 - \alpha^2\beta + 4\beta + 3\alpha + \alpha^3) \sinh \Delta + \frac{5}{3}\beta^2(2\beta^4 + 3\alpha\beta + 12\beta^2 + \alpha^3\beta - 9\alpha^2) \cosh \Delta - 10\alpha\beta^3 \quad (\text{A.9})$$

$$C_{10} = 2\beta^3(10\beta^4 + 5\alpha^3\beta + 48\beta^2 - 60\alpha^2 - 3\alpha^2\beta^2 + 15\alpha\beta + 60) \sinh \Delta - 2\beta^3(2\beta^5 + \alpha^3\beta^2 + 60\beta + 60\alpha + 3\alpha\beta^2 - 15\alpha^2\beta + 20\alpha^3 + 28\beta^3) \cosh \Delta + 24\alpha\beta^3(10 + 3\beta^2) \quad (\text{A.10})$$

$$C_{02} = (-3\alpha^2\beta + \alpha^3 + 3\alpha + 2\beta^3) \sinh \Delta + (-\alpha^3\beta + 3\alpha^2 - 3\alpha\beta - 2\beta^4) \cosh \Delta \quad (\text{A.11})$$

and

$$C_{00} = -2\beta^2(-\alpha^2\beta + \alpha^3 + 4\beta + 3\alpha + 2\beta^3) \sinh \Delta + \frac{2}{3}\beta^2(3\alpha\beta + \alpha^3\beta - 9\alpha^2 + 2\beta^4 + 12\beta^2) \cosh \Delta - 4\alpha\beta^3 \quad (\text{A.12})$$

$$B = \frac{1}{J} \left[ \frac{-B_0}{2(\alpha \sinh \beta - \cosh \alpha)} C + B_D D \right] \quad (\text{A.13})$$

where

$$B_0 = 3(\alpha^4 + 2\alpha\beta^3 + 3\alpha^2) \cosh \alpha + 9\alpha^2(\cosh \beta - \beta \sinh \beta - \alpha \sinh \alpha) + 3 \cosh \Delta [(\alpha^3 + 2\beta^3 + 3\alpha)(\alpha\beta \sinh \beta - \alpha \cosh \beta - \beta \cosh \alpha) + 3\alpha^2\beta \sinh \alpha] + 3 \sinh \Delta [(\alpha^3 + 2\beta^3 + 3\alpha) \cosh \alpha + 3\alpha^2(\alpha\beta \sinh \beta - \alpha \cosh \beta - \sinh \alpha)] \quad (\text{A.14})$$

and

$$B_D = \frac{5}{2}\beta^2[-(2\beta^4 + 12\beta^2 + 3\alpha\beta + \alpha^3\beta - 9\alpha^2)\cosh\Delta + 3(3\alpha + 4\beta + 2\beta^3 - \alpha^2\beta + \alpha^3)\sinh\Delta + 6\alpha\beta] \quad (\text{A.15})$$

$$H = \frac{H_C C + H_D D}{J} \quad (\text{A.16})$$

where

$$H_C = -[3(\alpha^3 + 2\beta^3)\cosh\alpha + 9\alpha(\cosh\alpha - \alpha\sinh\alpha - \cosh\beta + \beta\sinh\beta)] \quad (\text{A.17})$$

and

$$H_D = -15(3\alpha\beta^2\cosh\alpha - 3\alpha\beta^3\sinh\beta + 6\beta^3\cosh\alpha + 2\beta^5\cosh\alpha - 3\alpha\beta^2\cosh\beta + \alpha^3\beta^2\cosh\alpha - 3\alpha^2\beta^2\sinh\alpha) \quad (\text{A.18})$$

$$G = \frac{-3\alpha C - 15\alpha\beta^2 D - (\alpha\cosh\beta - \sinh\alpha)H}{\alpha\sinh\beta - \cosh\alpha} \quad (\text{A.19})$$

$$F = \frac{G\cosh\alpha + H\sinh\alpha}{3\alpha} \quad (\text{A.20})$$

$$E = 20\beta^3 D + 2B + 2\beta^3 F \quad (\text{A.21})$$

and

$$A = E - \beta^2 B - \beta^3 C - \beta^5 D + \beta^3 F + (\cosh\beta - \beta\sinh\beta)G + (\sinh\beta - \beta\cosh\beta)H = -\gamma^5 D \quad (\text{A.22})$$

Eq. (A.13) is then used to calculate  $\Omega$  of Eq. (25) and to plot Figs. 2 and 3.

### Nomenclature

$a$	radius of impermeable core
$\hat{a}$	dimensionless core radius, defined as $a/b$
$a_p$	radius of primary particle
$b$	radius of outer porous shell
$c$	radius of hypothetical cell
$D_f$	fractal dimension
$\mathbf{F}$	drag force experienced by a composite sphere
$k$	coefficient of Carman–Kozeny equation defined in Eq. (35)
$k_0$	prefactor of Eq. (44)
$N$	total number of primary particles in an aggregate
$p$	fluid pressure

$\Delta P$	pressure drop across membrane
$r$	radial coordinate
$r_c$	specific resistance of cake layer
$R_c$	cake resistance
$R_h$	hydrodynamic radius
$R_g$	gyration radius
$R_m$	membrane resistance
$u$	fluid velocity vector in spherical coordinate, i.e., $[u_r, u_\theta, u_\varphi]$
$v_s$	dimensionless settling velocity defined in Eq. (55)
$V$	approaching fluid velocity partially passing through composite sphere toward the membrane surface, i.e., permeate velocity

### Greek letters

$\alpha$	dimensionless solid sphere radius, defined as $a/\sqrt{\kappa}$
$\beta$	dimensionless outer shell radius, defined as $b/\sqrt{\kappa}$
$\gamma$	dimensionless hypothetical cell radius, defined as $c/\sqrt{\kappa}$
$\delta_c$	thickness of cake layer
$\varepsilon$	porosity of porous shell
$\eta$	dimensionless parameter, defined as $b/c (= \beta/\gamma)$
$\theta$	polar coordinate
$\kappa$	permeability
$\lambda$	occupancy fraction, defined as $\eta^3$
$\mu$	fluid viscosity
$\xi$	dimensionless radial coordinate, defined as $r/\sqrt{\kappa}$
$\rho_p$	mass density of primary particle
$\tau$	stress tensor
$\phi$	volume fraction
$\phi_{cs}$	radial profile of volume fraction of composite sphere
$\phi_{sh}$	volume fraction of porous shell of composite sphere
$\phi_0$	proportionality constant of Eq. (38)
$\langle\phi\rangle$	average volume fraction
$\varphi$	azimuthal coordinate
$\psi$	stream function
$\Omega$	dimensionless drag force defined in Eq. (24)
$\Omega_\infty$	dimensionless drag force in an infinitely dilute limit

### Subscripts

$B$	Brinkman
$c$	cake
$cs$	composite sphere
$CK$	Carman–Kozeny
$D$	Davies
$H$	Happel

NEN Neale, Epstein, and Nader  
 $r$  radial direction  
sh porous shell of composite sphere  
 $\theta$  angular direction

*Superscripts*

\* porous medium

## References

- [1] M.W. Chudacek, A.G. Fane, The dynamics of polarization in unstirred and stirred ultrafiltration, *J. Membrane Sci.* 21 (1984) 145–160.
- [2] J.G. Wijmans, S. Nakao, C.A. Smolders, Flux limitation in ultrafiltration—osmotic pressure model and gel layer model, *J. Membrane Sci.* 20 (1984) 115–124.
- [3] J.G. Wijmans, S. Nakao, J.W.A. Van Den Berg, F.R. Troelstra, C.A. Smolders, Hydrodynamic resistance of concentration polarization boundary layers in ultrafiltration, *J. Membrane Sci.* 22 (1985) 117–135.
- [4] C.A. Romero, R.H. Davis, Global model of crossflow microfiltration based on hydrodynamic particle diffusion, *J. Membrane Sci.* 39 (1988) 157–185.
- [5] C.A. Romero, R.H. Davis, Transient model of crossflow microfiltration, *Chem. Eng. Sci.* 45 (1990) 13–25.
- [6] C.A. Romero, R.H. Davis, Experimental verification of the shear-induced hydrodynamic diffusion model of crossflow microfiltration, *J. Membrane Sci.* 62 (1991) 249–273.
- [7] G. Belfort, R.H. Davis, A.L. Zydney, The behavior of suspensions and macromolecular solutions in crossflow microfiltration, *J. Membrane Sci.* 96 (1994) 1–58.
- [8] W.R. Bowen, F. Jenner, Theoretical descriptions of membrane filtration of colloids and fine particles—an assessment and review, *Adv. Colloid Interf. Sci.* 56 (1995) 141–200.
- [9] L.F. Song, M. Elimelech, Theory of concentration polarization cross-flow filtration, *J. Chem. Soc., Faraday Trans.* 91 (1995) 3389–3398.
- [10] S. Bhattacharjee, A. Sharma, P.K. Bhattacharya, A unified model for flux prediction during batch cell ultrafiltration, *J. Membrane Sci.* 111 (1996) 243–258.
- [11] M. Elimelech, S. Bhattacharjee, A novel approach for modeling concentration polarization in crossflow membrane filtration based on the equivalence of osmotic pressure model and filtration theory, *J. Membrane Sci.* 145 (1998) 223–241.
- [12] R.S. Faibish, M. Elimelech, Y. Cohen, Effect of interparticle electrostatic double layer interactions on permeate flux decline in crossflow membrane filtration of colloidal suspensions: an experimental investigation, *J. Colloid Interf. Sci.* 204 (1998) 77–86.
- [13] L. Song, A new model for the calculation of the limiting flux in ultrafiltration, *J. Membrane Sci.* 144 (1998) 173–185.
- [14] S. Bhattacharjee, A.S. Kim, M. Elimelech, Concentration polarization of interacting solute particles in cross-flow membrane filtration, *J. Colloid Interf. Sci.* 212 (1999) 81–99.
- [15] L. Song, Flux decline in crossflow microfiltration and ultrafiltration: mechanisms and modeling of membrane fouling, *J. Membrane Sci.* 139 (1998) 183–200.
- [16] E.M.V. Hoek, A.S. Kim, M. Elimelech, Influence of crossflow membrane filter geometry and shear rate on colloidal fouling in reverse osmosis and nanofiltration separations, *Environ. Eng. Sci.* 19 (2002) 357–372.
- [17] T.D. Waite, A.I. Schafer, A.G. Fane, A. Heuer, Colloidal fouling of ultrafiltration membranes: impact of aggregate structure and size, *J. Colloid Interf. Sci.* 212 (1999) 264–274.
- [18] F. Pignon, A. Magnin, J.-M. Piau, B. Cabane, P. Aimar, M. Meireles, P. Lindner, Structural characterisation of deposits formed during frontal filtration, *J. Membrane Sci.* 174 (2000) 189–204.
- [19] B. Cabane, M. Meireles, P. Aimar, Cake collapse in frontal filtration of colloidal aggregates: mechanisms and consequences, *Desalination* 146 (2002) 155–161.
- [20] K.-J. Hwang, H.-C. Liu, Cross-flow microfiltration of aggregated submicron particles, *J. Membrane Sci.* 201 (2002) 137–148.
- [21] D.A. Weitz, J.S. Huang, M.Y. Lin, J. Sung, Limits of the fractal dimension for irreversible kinetic aggregation of gold colloids, *Phys. Rev. Lett.* 54 (1985) 1416–1419.
- [22] P. Meakin, Diffusion-controlled cluster formation in two, three, and four dimensions, *Phys. Rev. A* 27 (1983) 604–607.
- [23] R. Jullien, Transparency effects in cluster–cluster aggregation with linear trajectories, *J. Phys. A* 17 (1984) L771–L776.
- [24] R. Jullien, M. Kolb, Hierarchical model for chemically limited cluster–cluster aggregates, *J. Phys. A* 17 (1984) L639–L643.
- [25] P. Meakin, F. Family, Structure and dynamics of reaction-limited aggregation, *Phys. Rev. A* 36 (1987) 5498–5501.
- [26] P. Meakin, F. Family, Structure and kinetics of reaction-limited aggregation, *Phys. Rev. A* 38 (1988) 2110–2123.
- [27] P. Meakin, Model for colloidal aggregation, *Ann. Rev. Phys. Chem.* 39 (1988) 237–267.
- [28] T.D. Waite, Measurement and implications of floc structure in water and wastewater treatment, *Colloids Surf. A: Physicochem. Eng. Aspects* 151 (1999) 27–41.
- [29] P.C. Carman, Fluid flow through a granular bed, *Trans. Inst. Chem. Eng.* 15 (1937) 150–156.
- [30] J. Happel, H. Brenner, *Low Reynolds Number Hydrodynamics*, Prentice-Hall, Englewood Cliffs, NJ, 1965.
- [31] A.S. Kim, E.M.V. Hoek, Cake structure in dead-end membrane filtration: Monte Carlo simulation, *Environ. Eng. Sci.* 19 (2002) 373–386.
- [32] G. Neale, N. Epstein, W. Nader, Creeping flow relative to permeable spheres, *Chem. Eng. Sci.* 28 (1973) 1865–1874.
- [33] S. Veerapaneni, M.R. Wiesner, Hydrodynamics of fractal aggregates with radially varying permeability, *J. Colloid Interf. Sci.* 177 (1996) 45–57.
- [34] A.S. Kim, K.D. Stolzenbach, The permeability of synthetic fractal aggregates with realistic three-dimensional structure, *J. Colloid Interf. Sci.* 253 (2002) 315–328.
- [35] J. Happel, Viscous flow in multiparticle systems: slow motion of fluids relative to beds of spherical particles, *AIChE J.* 4 (1958) 197–201.
- [36] H.C. Brinkman, Problems of fluid flow through swarms of particles and through macromolecules in solution, *Research (London)* 2 (1949) 190–194.
- [37] J.H. Masliyah, G. Neale, Creeping flow over a composite sphere: solid core with porous shell, *Chem. Eng. Sci.* 42 (1987) 245–253.
- [38] G. Ooms, P.F. Mijnlieff, H. Beckers, Friction force exerted by a flowing fluid on a permeable particle, with particular reference to polymer coils, *J. Chem. Phys.* 53 (1970) 4123–4130.
- [39] K.D. Stolzenbach, Scavenging of small particles by fast-sinking porous aggregates, *Deep-Sea Res.* 40 (1993) 359–369.
- [40] T.S. Lundgren, Slow flow through stationary random beds and suspensions of spheres, *J. Fluid Mech.* 51 (1972) 229–273.
- [41] P.G. Saffman, On the boundary condition at the surface of a porous medium, *Stud. Appl. Math.* 50 (1971) 93–101.
- [42] S. Haber, R. Mauri, Boundary conditions for Darcy's flow through porous media, *Int. J. Multiphase Flow* 9 (1983) 561–574.
- [43] J. Koplik, L. Herbert, A. Zee, Viscosity renormalization in Brinkman equation, *Phys. Fluids* 26 (1983) 2864–2870.
- [44] H.C. Brinkman, A calculation of the viscous force exerted by a flowing fluid on a dense swarm of particles, *Appl. Sci. Res. A* 1 (1947) 27–34.

- [45] A.G. Fane, Ultrafiltration of suspensions, *J. Membrane Sci.* 20 (1984) 249–259.
- [46] P. Bacchin, P. Aimar, V. Sanchez, Influence of surface interaction on transfer during colloid ultrafiltration, *J. Membrane Sci.* 115 (1996) 49–63.
- [47] L. Wang, L. Song, Flux decline in crossflow microfiltration and ultrafiltration: experimental verification of fouling dynamics, *J. Membrane Sci.* 160 (1999) 41–50.
- [48] A.L. Alldredge, C. Gotschalk, In situ settling behavior of marine snow, *Limnol. Oceanogr.* 33 (1988) 339–351.
- [49] B.E. Logan, D.B. Wilkinson, Fractal geometry of marine snow and other biological aggregates, *Limnol. Oceanogr.* 35 (1990) 130–136.
- [50] C.P. Johnson, X. Li, B.E. Logan, Settling velocities of fractal aggregates, *Environ. Sci. Technol.* 30 (1996) 1911–1918.
- [51] X. Li, B.E. Logan, Collision frequencies of fractal aggregates with small particles by differential sedimentation, *Environ. Sci. Technol.* 31 (1997) 1229–1236.
- [52] X. Li, B.E. Logan, Collision frequencies between fractal aggregates and small particles in a turbulently sheared fluid, *Environ. Sci. Technol.* 31 (1997) 1237–1242.
- [53] K.-J. Hwang, H.-C. Liu, W.-M. Lu, Local properties of cake in cross-flow microfiltration of submicron particles, *J. Membrane Sci.* 138 (1998) 181–192.
- [54] S.N. Rogak, R.C. Flagan, Stokes drag on self-similar clusters of spheres, *J. Colloid Interf. Sci.* 134 (1990) 206–218.
- [55] S.N. Rogak, R.C. Flagan, Coagulation of aerosol agglomerates in the transition regime, *J. Colloid Interf. Sci.* 151 (1992) 203–224.
- [56] C.M. Sorensen, G.C. Roberts, The prefactor of fractal aggregates, *J. Colloid Interf. Sci.* 186 (1997) 447–452.
- [57] C.N. Davies, The separation of airborne dust and particles, *Proc. Inst. Mech. Engrs. B* 1 (1952) 185–213.
- [58] Z.-Y. Chen, P. Meakin, J.M. Deutch, Comment on “hydrodynamic behavior of fractal aggregates”, *Phys. Rev. Lett.* 59 (1987) 2121.
- [59] W. Soppe, Computer simulation of random packings of hard spheres, *Powder Technol.* 62 (1990) 189–196.
- [60] G.T. Nolan, P.E. Kavanagh, Computer simulation of random packing of hard spheres, *Powder Technol.* 72 (1992) 149–155.
- [61] G.Y. Onoda, E.G. Liniger, Random loose packing of uniform spheres and the dilatancy onset, *Phys. Rev. Lett.* 64 (1990) 2727–2730.